Atmos. Chem. Phys. Discuss., 12, 33443–33488, 2012
www.atmos-chem-phys-discuss.net/12/33443/2012/
doi:10.5194/acpd-12-33443-2012

Atmospheric Chemistry and Physics Discussions

Net radiative forcing and air quality responses to regional CO emission reductions

M. M. Fry[1], **M. D. Schwarzkopf**[2], **Z. Adelman**[1], **V. Naik**[3], **W. J. Collins**[4], **and J. J. West**[1]

[1]Department of Environmental Sciences and Engineering, University of North Carolina at Chapel Hill, Chapel Hill, North Carolina, USA
[2]NOAA Geophysical Fluid Dynamics Laboratory, Princeton, New Jersey, USA
[3]UCAR/NOAA Geophysical Fluid Dynamics Laboratory, Princeton, New Jersey, USA
[4]Department of Meteorology, University of Reading, Reading, UK

Received: 24 November 2012 – Accepted: 5 December 2012 – Published: 21 December 2012

Correspondence to: J. J. West (jjwest@email.unc.edu)

Published by Copernicus Publications on behalf of the European Geosciences Union.

Abstract

Carbon monoxide (CO) emissions influence global and regional air quality and global climate change by affecting atmospheric oxidants and secondary species. We simulate the influence of halving anthropogenic CO emissions globally and individually from 10 regions on surface and tropospheric ozone, methane, and aerosol concentrations using a global chemical transport model (MOZART-4 for the year 2005). Net radiative forcing (RF) is then estimated using the GFDL standalone radiative transfer model. We estimate that halving global CO emissions decreases global annual average concentrations of surface ozone by 0.45 ppbv, tropospheric methane by 73 ppbv, and global annual net RF by 36.1 $mW\,m^{-2}$, nearly equal to the sum of changes from the 10 regional reductions. Global annual net RF per unit change in emissions and the 100-yr global warming potential (GWP_{100}) are estimated as $-0.124\,mW\,m^{-2}\,(Tg\,CO\,yr^{-1})^{-1}$ and 1.34, respectively, for the global CO reduction, and ranging from −0.115 to $-0.131\,mW\,m^{-2}\,(Tg\,CO\,yr^{-1})^{-1}$ and 1.26 to 1.44 across 10 regions, with the greatest sensitivities for regions in the tropics. The net RF distributions show widespread cooling corresponding to the O_3 and CH_4 decreases, and localized positive and negative net RFs due to changes in aerosols. The strongest annual net RF impacts occur within the tropics (28° S–28° N) followed by the northern mid-latitudes (28° N–60° N), independent of reduction region, while the greatest changes in surface CO and ozone concentrations occur within the reduction region. Some regional reductions strongly influence the air quality in other regions, such as East Asia, which has an impact on US surface ozone that is 93 % of that from North America. Changes in the transport of CO and downwind ozone production clearly exceed the direct export of ozone from each reduction region. The small variation in CO GWPs among world regions suggests that future international climate agreements could adopt a globally uniform metric for CO with little error, or could use different GWPs for each continent. Doing so may increase the incentive to reduce CO through coordinated policies addressing climate and air quality.

ACPD
12, 33443–33488, 2012

1 Introduction

Carbon monoxide (CO) is emitted from the incomplete combustion of carbon fuels, and contributes indirectly to climate change through its influence on tropospheric ozone (O_3) and atmospheric oxidants (e.g. hydroxyl radical [OH], hydrogen peroxide [H_2O_2], O_3), which in turn affect the abundance of methane (CH_4) and aerosols (Pham et al., 1995; Unger et al., 2006; Shindell et al., 2009). CO emission reductions impact both climate and air quality by increasing tropospheric OH concentrations, which lead to decreases in global CH_4 abundance and thus, long-term O_3 (Prather et al., 1996; Wild et al., 2001; Fiore et al., 2002; Naik et al., 2005), as CH_4 is a longer-lived precursor to tropospheric O_3 (West et al., 2007, 2009a; Fiore et al., 2009). Here, we assess the net climate impact of reducing anthropogenic CO emissions globally and from 10 world regions individually, to inform future policies that may address air quality and climate jointly.

Tropospheric O_3 and CH_4, both greenhouse gases, have contributed abundance-based anthropogenic radiative forcings (RF) of $0.35\,[-0.1, +0.3]\,W\,m^{-2}$ and $0.48 \pm 0.05\,W\,m^{-2}$, respectively, the largest greenhouse gas forcings behind CO_2 (Forster et al., 2007). CO and volatile organic compounds (VOC) emissions provide important contributions toward these forcings, estimated as $0.21 \pm 0.10\,W\,m^{-2}$ due to tropospheric O_3 and CH_4 changes (Shindell et al., 2005; Forster et al., 2007), and $0.25 \pm 0.04\,W\,m^{-2}$ (from 1750 to 2000) when the effects on sulfate and nitrate aerosols and CO_2 are included (Shindell et al., 2009).

In addition to being near-term climate forcers, products of CO reactions (O_3 and aerosols) are important air pollutants. CO emissions not only affect O_3 concentrations locally, but also intercontinentally (Akimoto, 2003; TF HTAP, 2010), given tropospheric ozone's mean lifetime of 22 days (Stevenson et al., 2006) and CO's lifetime of one to three months, both of which exceed typical intercontinental transport times (5 to 10 days) (Fiore et al., 2009; West et al., 2009a). Because of its lifetime, the transport of CO makes an important contribution to long-range O_3 (Heald et al., 2003). However,

ACPD
12, 33443–33488, 2012

recent studies have identified large uncertainties in regional CO emissions inventories (Duncan et al., 2007), compared to satellite data (Heald et al., 2004; Pétron et al., 2004; Pfister et al., 2004, 2005; Kopacz et al., 2009), e.g. underestimating tropical biomass burning emissions and northern mid-latitude seasonal variation in bottom-up inventories (Kopacz et al., 2010). CO emissions also affect atmospheric aerosols including sulfate (SO_4^{2-}) by influencing the oxidation of sulfur dioxide (SO_2) by OH in the gas phase, or by H_2O_2 or O_3 in the aqueous phase. OH increases from CO reductions lead to increased gas-phase SO_4^{2-} formation, and hence, climate cooling, while H_2O_2 and O_3 decreases lead to decreased aqueous-phase SO_4^{2-} formation (locally to intercontinentally) and climate warming (Unger et al., 2006; Leibensperger et al., 2011). In addition, CO influences the abundance of ammonium nitrate (NH_4NO_3) and secondary organic aerosols (SOA) via oxidant changes (Bauer et al., 2007; Hoyle et al., 2009).

For more than a decade, many have suggested that short-lived climate forcers and their precursors, like CO, be considered in international climate agreements, in addition to national air quality programs (Fuglestvedt et al., 1999; Rypdal et al., 2005, 2009; Naik et al., 2005; Fry et al., 2012), and it is among these short-lived climate forcers for which reducing emissions can slow the near-term rate of climate change (Jackson, 2009; Shindell et al., 2012). One reason why CO has not been included in a climate mitigation strategy is that its RF varies by region of emissions, given its relatively short lifetime in the troposphere (Berntsen et al., 2005). Global warming potentials (GWP) have been estimated for global CO emissions, with values ranging from 1.0 to 3.0 for a 100-yr time horizon (GWP_{100}) (Fuglestvedt et al., 1996; Johnson and Derwent, 1996; Daniel and Solomon, 1998; Collins et al., 2002), based on O_3 production and feedbacks on CH_4. Few studies have estimated GWPs for CO emissions from particular world regions. Berntsen et al. (2005) estimated GWPs for CO emissions from Europe and Southeast Asia, finding that the GWP for Asian CO emissions was 25 % higher than that for European emissions. Fry et al. (2012) also calculated CO GWP estimates for four world regions using an ensemble of global models, showing a small range (GWP_{20}: 4.6 ± 1.3 to 5.3 ± 1.2; GWP_{100}: 1.5 ± 0.4 to 1.7 ± 0.5) with coefficients

ACPD
12, 33443–33488, 2012

of variation (CV = standard deviation/mean) of 0.065 for GWP_{20} and 0.059 for GWP_{100}, where the European reduction produced a lower GWP than North America, East Asia, and South Asia reductions. Further research on the sensitivity of net RF and CO GWPs to the region of CO emissions, including regions within the tropics and Southern Hemisphere (SH), may inform future policies that address climate change over the next 30 yr, in coordination with longer-term CO_2 mitigation (Daniel and Solomon, 1998; Shindell et al., 2012).

In this paper, we evaluate the effects of 50 % anthropogenic CO emission reductions from 10 regions individually, and globally, on stratospheric-adjusted net RF, tropospheric burdens (O_3, CH_4, and aerosols), and surface O_3 air quality to inform future coordinated actions addressing air quality and climate. We simulate the influence of CO emission reductions on tropospheric chemical composition using a global chemical transport model (CTM) and then apply a standalone radiative transfer model (RTM) to estimate the RF from changes in O_3, CH_4, and the direct effect of aerosols. We present the variability in CO RF and GWPs from 10 regions, while previous studies only evaluated CO emissions perturbations from a few regions (Berntsen et al., 2005; Fiore et al., 2009; TF HTAP, 2010; Fry et al., 2012). The global annually averaged net RF estimates given here are indicators of global mean surface temperature changes, but do not account for regional climate changes from spatially nonuniform forcings (Shindell et al., 2009).

2 Methods

2.1 Chemical transport modelling

Using the Model for Ozone and Related chemical Tracers, version 4 (MOZART-4) (Emmons et al., 2010), we simulate anthropogenic CO emission reductions from 10 regions (North America [NA], South America [SA], Europe [EU], Former Soviet Union [FSU], Africa [AF], India [IN], East Asia [EA], Southeast Asia [SE], Australia and New Zealand

ACPD
12, 33443–33488, 2012

[AU], and Middle East and Northern Africa [ME]) (Fig. 1) and globally (sum of emissions from 10 regions only), relative to a base simulation. We use the Coupled Model Intercomparison Project Phase 5 (CMIP5) Representative Concentration Pathway 8.5 (RCP8.5) emissions inventory for the year 2005 (Riahi et al., 2007, 2011) and global meteorology from the Goddard Earth Observing System Model, version 5 (GEOS-5) for the years 2004 to 2006 (Rienecker et al., 2008) as inputs to MOZART-4.

The RCP8.5 volatile organic compound (VOC) species are re-speciated to MOZART-4 VOC categories by matching like species. Monthly temporal variation is added to all emissions species from anthropogenic sources, in each grid cell, by scaling to the monthly profile of emissions species in the REanalysis of the TROpospheric chemical composition over the past 40 yr (RETRO) global emissions dataset (Schultz et al., 2007), while shipping, aircraft, and biomass burning emissions already have monthly temporal variation. Biogenic emissions of isoprene and monoterpenes are calculated online in MOZART-4 using the Model of Emissions of Gases and Aerosols from Nature (MEGAN) (Guenther et al., 2006), based on the methods of Pfister et al. (2008), while all other natural emissions are taken from the Precursors of Ozone and their Effects in the Troposphere (POET) emissions inventory for the year 2000 (Olivier et al., 2003; Granier et al., 2005; Emmons et al., 2010).

The global and regional reduction simulations are run from 1 July 2004 through 31 December 2005 at 1.9° × 2.5° (latitude × longitude) horizontal resolution and 56 vertical levels. The base simulation is run through December 31, 2006 to allow for further comparisons with observations. Global CH_4 is set to a uniform mixing ratio of 1783 parts per billion by volume (ppbv) (WMO, 2006) in the base and perturbed simulations given their short duration (1.5 yr), and an additional CH_4 control simulation reduces global CH_4 by 20 % to 1426.4 ppbv. Using the results from the base and CH_4 control simulations, we estimate CH_4 lifetime against loss by tropospheric OH (τ_{OH}, 11.24 yr), total CH_4 lifetime based on τ_{OH} and CH_4 loss to soils and the stratosphere (τ_{total}, 9.66 yr), and methane's feedback factor (F, 1.29) by the methods of Prather et al. (2001), finding that our τ_{OH} is slightly higher than those estimated by Fiore et al. (2008) (10.3 yr) and Emmons

ACPD
12, 33443–33488, 2012

et al. (2010) (10.5 yr), but within the range of other models: 8.2 to 11.7 yr (Stevenson et al., 2006), 10.2 ± 1.7 yr (Fiore et al., 2009), and 9.8 ± 1.6 yr (Voulgarakis et al., 2012). Prather et al. (2012) also recently estimated τ_{OH} as 11.2 ± 1.3 yr based on observations. Using our calculated parameters, we diagnose changes in global CH_4 burden for each perturbation. We then calculate long-term O_3 responses offline, by scaling the change in O_3 from the CH_4 control simulation (CH_4 control simulation minus base) in each grid cell by the ratio of global CH_4 burden change from each perturbation to that of the CH_4 control simulation. Long-term O_3 responses are added to the short-term O_3 responses simulated directly for each CO emission reduction (described below) to yield O_3 concentrations at steady state (West et al., 2007; Fiore et al., 2009; Fry et al., 2012).

MOZART-4 simulates the tropospheric aerosols SO_4^{2-}, black carbon (BC), organic carbon (OC), primary and secondary organics, NH_4NO_3, and sea salt aerosols (Lamarque et al., 2005; Emmons et al., 2010). Here we quantify the changes in SO_4^{2-}, NH_4NO_3, and SOA, as these aerosols are most directly influenced by anthropogenic CO emissions via changes in oxidants. SO_4^{2-} aerosols in MOZART-4 are produced from SO_2 and dimethylsulfide (DMS) emissions through gas and aqueous-phase oxidation (Barth et al., 2000), while NH_4NO_3 aerosols are calculated from the oxidation of nitrogen oxides (NO_x) to nitric acid (HNO_3), and subsequent reaction with NH_3 emissions (Metzger et al., 2002). SOA is formed through the gas-phase oxidation of monoterpenes by OH, O_3, and nitrate (NO_3), and the gas-phase oxidation of toluene by OH (Chung and Seinfeld, 2002).

Each perturbation simulation reduces anthropogenic CO emissions by 50 % in one region (or globally), while leaving all other emissions unchanged. Figure 2 shows the total anthropogenic CO emissions by region and sector for the base simulation. Anthropogenic CO emissions include all source categories in Fig. 2, but exclude biomass burning (except for the agriculture and waste burning categories), such as forest fires and grassland fires, which are also large sources of CO. We exclude biomass burning as actions to address biomass burning differ from the other sectors addressed here,

ACPD
12, 33443–33488, 2012

and would reduce a suite of emissions simultaneously (Naik et al., 2007). Using the global, three-dimensional results from each perturbation, global and regional changes in air quality (O_3 and aerosols) at the surface (within the first vertical level) and across the troposphere (region with O_3 levels less than 150 ppbv) are quantified, relative to the base simulation, including the influence of each regional reduction on O_3 long-range transport.

2.2 MOZART-4 evaluation

Previous MOZART-4 simulations, with comparable model formulations but different inputs, have reproduced O_3 and CO observations well (e.g. Pfister et al., 2005, 2006; Lapina et al., 2006; Horowitz et al., 2007; Pfister et al., 2008; Emmons et al., 2010). Table 1 summarizes the total anthropogenic CO emissions and annual average surface O_3, SO_4^{2-}, and CO concentrations regionally and globally for the base simulation. The base simulation produces an average bias of 4.5 ppbv O_3 across all sites compared to the Clean Air Status and Trends Network (CASTNET) (Fig. S1), and 0.8 ppbv O_3 compared to the European Monitoring and Evaluation Programme (EMEP) network (Fig. S2). Simulated annual average surface SO_4^{2-} concentrations are mostly within a factor of two of observations from the Interagency Monitoring of Protected Visual Environments (IMPROVE) and EMEP monitoring networks for 2005 (Fig. S3). The base simulated monthly mean surface CO concentrations also generally agree with the seasonal cycle of NOAA CMDL surface CO measurements, but overestimate CMDL measurements in the SH (Fig. S4), as was also found by Emmons et al. (2010).

Simulated monthly 2005 and 2006 vertical O_3 profiles are comparable to 1995 to 2009 monthly mean and median ozonesonde climatology (Tilmes et al., 2012) (Fig. S5), with the greatest agreement at 800 and 500 millibar (mb) altitudes (Fig. S6). Larger differences exist between the base simulated O_3 and ozonesonde climatology at 200 mb, which may reflect the model's upper boundary conditions and constraints (Emmons et al., 2010).

ACPD
12, 33443–33488, 2012

Our base 2005 simulated OH burdens are lower than Spivakovsky et al. (2000), but fairly comparable to those of Lawrence (1996), Lawrence et al. (1999), von Kuhlmann (2001), and Emmons et al. (2010) (Table S1). The percentage loss of tropospheric CH_4 by reaction with OH in the base simulation is comparable to Fiore et al. (2008) (Table S2), yet slightly lower in the lower troposphere (surface to 750 hPa), and slightly higher in the mid and upper troposphere (750 to 250 hPa).

2.3 Radiative transfer modelling

The NOAA Geophysical Fluid Dynamics Laboratory (GFDL) RTM is used to estimate the stratospheric-adjusted net RF due to changes in tropospheric steady-state O_3, CH_4, and SO_4^{2-}aerosols (direct effect). The GFDL RTM is a module of the GFDL coupled atmosphere-ocean model (AM2) and simulates solar and infrared radiative transfer (GFDL GAMDT, 2004; Naik et al., 2005, 2007). This RTM has been applied in studies of long-lived greenhouse gases (Schwarzkopf and Ramaswamy, 1999) and short-lived forcing agents (Naik et al., 2005, 2007; West et al., 2007; Fiore et al., 2008; Saikawa et al., 2009; Fry et al., 2012). Here the RTM is employed as in Fry et al. (2012) at 144 × 90 × 24 levels, and with updated well-mixed greenhouse gas concentrations including CO_2 and nitrous oxide (N_2O) (Meinshausen et al., 2011) and CMIP5 solar forcing data (http://www.geo.fu-berlin.de/en/met/ag/strat/forschung/SOLARIS/Input_data/CMIP5_solar_irradiance.html). The RTM simulations do not include the indirect effects of aerosols on clouds or the internal mixing of aerosols. Changes in the RF contributions from nitrate aerosols, stratospheric O_3, water vapor, the carbon cycle via O_3 and nitrogen deposition, and CO_2 (from changes in CH_4 and CO oxidation) are excluded. CO oxidizes to CO_2 in the atmosphere, with a minor influence on the net RF of CO (Shindell et al., 2009). Since this carbon is likely already accounted for in inventories of CO_2, we do not estimate CO_2 forcing here (Daniel and Solomon, 1998).

Tropospheric O_3, CH_4, SO_4^{2-}, BC, and OC concentrations from the MOZART-4 base and perturbed simulations are used as inputs to the RTM simulations, along with

ACPD
12, 33443–33488, 2012

meteorological fields from GFDL's atmosphere model (AM2) and land model (LM2), sampled one day per month at midmonth for the year 2005, to represent monthly mean conditions (Naik et al., 2005). BC and OC concentrations are not evaluated further as changes in these species between the base and perturbed simulations are negligible, but we include them as inputs to the RTM simulations. The RTM currently does not calculate the RF of SOA and NH_4NO_3 aerosols. The net RF is calculated as the difference between the perturbed and base cases' simulated monthly mean net radiation fluxes (net shortwave minus net longwave), in each grid cell and month, at the tropopause after allowing stratospheric temperatures to readjust to radiative equilibrium (Naik et al., 2007; Saikawa et al., 2009; Fry et al., 2012).

3 Global and regional air quality responses

3.1 Surface CO concentrations

We first analyze the magnitude and distribution of annual average surface CO concentrations for each 50 % reduction in anthropogenic CO emissions, relative to the base. Figure 3 shows that the largest decreases in surface CO occur within each reduction region, with lesser decreases intercontinentally. The foreign region that most influences the US is EA, which contributes 39 % of the change in US surface CO that results from the NA reduction (Table 2). Responses normalized by emission change are listed in Table S3.

3.2 Responses of methane and ozone

3.2.1 Tropospheric methane

Changes in global tropospheric steady-state CH_4 abundance for each perturbation relative to the base are calculated using the tropospheric CH_4 loss flux diagnosed from the model (West et al., 2007; Fiore et al., 2009; Fry et al., 2012) (Table 3). The EA reduction

ACPD
12, 33443–33488, 2012

produces the greatest change in global CH_4 (−19.4 ppbv), followed by IN (−11.5 ppbv) and AF (−10.9 ppbv) reductions. Upon normalizing by the change in CO emissions, global CH_4 varies little among regions (CV = 0.054), suggesting that the sensitivity of global CH_4 to CO emissions is nearly independent of emission region (Fig. S7, Table S9). Fry et al. (2012) also found that CH_4 sensitivity to CO emission changes varies little (0.22 to 0.24 ppbv CH_4 $(Tg\,CO)^{-1}$), in contrast to the more regionally-variable effects of NO_x and NMVOC emissions on CH_4.

3.2.2 Surface and tropospheric ozone

Global CH_4 changes are used to calculate long-term, tropospheric O_3 changes, which are added to short-term changes to give steady-state O_3 responses (Table 4). Steady-state global O_3 changes are 40 to 83 % greater than short-term changes, suggesting that the long-term influence of CO via CH_4 is relevant for air quality (West et al., 2007). Both short-term and steady-state global surface O_3 responses are approximately proportional to the level of CO emissions change (Fig. S10). In addition, estimated changes in long-term O_3 per unit CO emissions vary little among regions. Values in Table 4 could be scaled to other emissions changes, allowing long-term effects to be included in future global or regional modeling exercises (e.g. West et al., 2009b for NO_x).

Surface O_3 responses are greatest within the hemisphere of reduction; since inter-hemispheric transport takes about 1 yr, little mixing occurs across hemispheres (Jacob, 1999; West et al., 2009a). The long-term O_3 component (via CH_4), however, impacts air quality globally. The distributions of steady-state surface O_3 changes are shown in Fig. 4, and are quantified as annual average changes within all 10 regions and the US (Table 5). The greatest steady-state surface O_3 decreases occur within the reduction region, with smaller decreases hemispherically, except for the AU reduction, which has little effect (< 2.1 pptv) on foreign regions (Table 5). Similar trends are seen in regional steady-state surface O_3 responses normalized per unit change in CO emissions (Table S4).

ACPD
12, 33443–33488, 2012

The sum of global annual mean steady-state surface O_3 changes from the 10 regional reductions (−448 pptv) is nearly equivalent to that of the global CO reduction (−450 pptv). However, steady-state surface O_3 (normalized per unit change in CO emissions) is most sensitive to FSU and EU reductions (−2.1 and −2.0 pptv/Tg CO yr^{-1}, respectively) (Table 4). The largest CO emitters (EA, IN, AF, and NA) (Table 1) produce the greatest impacts within the reduction region or between regions. EA is the foreign region that most influences the US, with an influence on surface O_3 that is nearly as large (93 %) as the influence from NA CO emissions. Reducing NA CO emissions strongly impacts EU and ME surface O_3, with an influence that is 77 % and 75 %, respectively, of domestic impacts. In some cases, foreign CO emission reductions have a greater impact on O_3 than a region's own domestic reduction, such as EA which reduces surface O_3 in EU by 22 % more than the EU reduction (Table 5). As in Fiore et al. (2009), for NH sources and receptors, the greatest transport and intercontinental influences of each region on other regions are mainly from March to June (Fig. S11).

The distributions of steady-state tropospheric total column O_3 changes (Fig. 5) are similar to surface O_3 responses (Fig. 4), yet more widespread hemispherically to globally. The troposphere is defined for O_3 less than 150 ppbv, and the upper troposphere (UT) from 500 hPa to the tropopause. We distinguish between full troposphere and UT O_3 burdens, since O_3 in the UT has a higher RF efficiency per molecule (Lacis et al., 1990; Wang et al., 1993; Forster and Shine, 1997). The EA reduction has the strongest impact on total column O_3 across the NH, while the AU CO reduction has the least impact on total column O_3 globally. Tropospheric total column O_3 changes are less than 2 % in all locations, for each perturbation (Fig. S12). Normalized global annual mean full and UT steady-state O_3 burden changes (Table S5) are greatest for SE, IN, and AF reductions, due to the stronger photochemistry and more active vertical convection in the tropics.

ACPD
12, 33443–33488, 2012

3.2.3 Response of aerosols

Tropospheric annual mean burden changes in SO_4^{2-}, NH_4NO_3, and SOA are presented in Table 3. The IN, ME, and AF reductions increase global SO_4^{2-} burden, while all other perturbations decrease global SO_4^{2-}. Global NH_4NO_3 burden also increases and decreases across the regional perturbations, but the global SOA burden decreases in all cases. The oxidation of SO_2, NO_x, monoterpenes, and toluene depend on the availability of atmospheric oxidants. Increases in OH are expected to increase the global annual average SO_4^{2-}, NH_4NO_3, and SOA burdens, while decreases in O_3 (and H_2O_2 for SO_2 oxidation) are expected to decrease the global annual average SO_4^{2-} and SOA burdens.

Most regional perturbations show stronger increases in tropospheric OH within the source region, and smaller, widespread increases in the tropics (30° S to 30° N) (Fig. S13). Tropospheric total column H_2O_2 changes are opposite in sign, with the greatest decreases within the reduction region and extending longitudinally (Fig. S14).

In Fig. 6, annual average tropospheric total column SO_4^{2-} changes result from several SO_2 oxidation pathways, where CO's lifetime is long enough that the resulting SO_4^{2-} patterns are fairly independent of reduction region. In the northern mid-latitudes, SO_4^{2-} decreases likely relate to the prevalence of clouds and decreased aqueous-phase SO_2 oxidation (in clouds) by O_3 and H_2O_2. Near the equator and in drier regions (i.e. near ME and AF), gas-phase SO_2 oxidation by OH dominates, leading to increases in SO_4^{2-}. The greatest total column SO_4^{2-} percentage decreases (i.e. for NA, EU, and EA reductions) and greatest SO_4^{2-} percentage increases (i.e. for AF, IN, EA, and ME reductions) over the reduction region are 2 % or less. Intercontinental to hemispheric effects are generally 0.1 % or less, for all regional reductions (Fig. S15). Our regional annual average surface $PM_{2.5}$ changes (0.059 $\mu g\,m^{-3}$ or less) are only slightly smaller than those estimated by Leibensperger et al. (2011) ($\sim$0.1 $\mu g\,m^{-3}$ from Asian NO_x and CO on northern Europe and eastern China, and $\sim$0.25 $\mu g\,m^{-3}$ from US NO_x and CO on

ACPD
12, 33443–33488, 2012

northern Europe and eastern China) who zeroed-out anthropogenic emissions, while we halve them here. CO generally does not have a strong influence on $PM_{2.5}$ air quality in our simulations.

4 Changes in production and export of CO and ozone

SA, EU, FSU, and AU reductions produce the greatest changes in global CO burden per unit change in CO emissions, and also result in the longest CO lifetimes (82 to 94 days) (Table 6, Table S9). More than 79 % of CO burden changes occur outside of the reduction region for all perturbations, and between 41 % and 50 % of CO burden changes take place in the UT for SE, SA, AF, and IN reductions, consistent with the regions that have the greatest impact on O_3 production in the UT (Table 7). We find decreases in CO export from the reduction region in all cases, and increases in global CO production. These increases in CO production ($\sim$ 2 % for the global CO reduction) result from tropospheric OH increases that cause faster oxidation of CH_4 and non-methane volatile organic compounds (NMVOCs) (Shindell et al., 2006). However, the global CO loss frequency (or inverse lifetime) (Prather et al., 2012) increases by $\sim$ 3.4 % for the global CO reduction, indicating that as CO is reduced, increases in OH lead to further CO loss. Therefore in this study, the CO perturbation lifetime ($\Delta B_{CO}/\Delta E_{CO}$) is slightly greater than the CO atmospheric lifetime ($B_{CO}/(E_{COanthro} + E_{COnatural} + P_{CO})$) (feedback factor of $\sim$ 1.06), which suggests that perturbing CO emissions can have an overall amplifying effect. Although we do not account for the long-term effects on CH_4 directly in our 1.5-yr simulations, these can be calculated offline from the changes in CH_4 lifetime as was done for O_3. Global CH_4 decreases also lead to decreases in CO production at steady state, and furthermore, increases in OH that cause increases in CO loss and production. These are summarized in Table S9. The long-term changes further amplify the CO signal leading to a total increase in CO loss frequency of $\sim$ 4.5 %, and a total feedback factor $(\Delta B_{CO}/B_{CO})/(\Delta E_{CO}/(E_{CO} + P_{CO}))$ of 1.19.

ACPD
12, 33443–33488, 2012

O_3 production and export changes are also calculated for each regional reduction to determine whether the transport of O_3 or CO is more important for long-range O_3. Table 7 shows that the change in short-term tropospheric O_3 burden per unit change in CO emissions (Table S9 shows steady-state burden changes) is most sensitive to SE, IN, and AF reductions, which agrees with previous studies showing greater sensitivity of O_3 (especially in the mid- to upper troposphere) to emissions from the tropics, compared to more temperate regions (Fuglestvedt et al., 1999; Berntsen et al., 2005; Naik et al., 2005; West et al., 2009b). In the tropics, stronger photochemistry enhances O_3 and more active convection increases the transport of O_3 and CO to the UT, where O_3 lifetimes are longer (Naik et al., 2005; West et al., 2009b). Table 7 also shows that SE, SA, AF, and IN reductions produce the highest fractions of change in global O_3 production in the UT (above 500 hPa) (between 50 % and 59 %), suggesting that these regions also produce the greatest changes in the vertical convection of CO to the UT. As in West et al. (2009a), the higher water vapor concentrations and convective mixing in the tropics, which would lead to shorter O_3 lifetimes than at higher latitudes (Lawrence et al., 2003), appear to be less important, as CO reductions near the tropics have the greatest influence on global O_3 burden and production.

For all of the regional reductions, more than 70 % of the changes in global O_3 burden and global O_3 production occur outside the reduction region, with changes in O_3 production (ΔP) outside the reduction region greatly exceeding changes in O_3 export (ΔX) (Table 7). This demonstrates that the downwind production of O_3 from CO is more important for long-range O_3 transport than the direct formation and export of O_3 from CO within each source region. This differs from the case of NO_x for which changes in O_3 export exceed changes in O_3 production downwind (West et al., 2009a), reflecting the longer lifetime of CO compared to NO_x.

ACPD
12, 33443–33488, 2012

5 Radiative forcing and global warming potentials

The stratospheric-adjusted net RF impacts for the combined effect of tropospheric O_3, CH_4, and SO_4^{2-} concentration changes are shown in Fig. 7 and Table 8. Annual average net RF distributions show widespread cooling (negative net RFs) across the NH and SH, for all of the regional (and global) CO reductions (Fig. 7), due to global decreases in CH_4 (and long-term O_3) and regional to hemispheric decreases in short-term O_3. Localized to regional cooling and warming patterns, especially from the NA, EU, FSU, and EA reductions, correspond to localized increases and decreases in SO_4^{2-} aerosols (Fig. 6, Fig. 7). The large-scale influences of CH_4 and O_3 are consistent with the long-wave radiation distributions (Fig. S17), while the local influences of SO_4^{2-} are reflected in the shortwave radiation distributions (Fig. S18). The strongest annual average net RFs occur within the 28° S to 28° N latitudinal band in all cases (Table 8), despite the wide range of reduction regions. This finding is explained by the hotter surface temperatures in the tropics, which result in greater outgoing longwave radiation absorption by greenhouse gases. However, longwave forcings are not as strong directly over the equator, since water vapor is abundant and competes with O_3 absorption in this region (Fig. S17).

Across all 10 regional reductions, the global annual net RF per unit emissions is $-0.12 \pm 0.0055\,\mathrm{mW\,m^{-2}}\ (\mathrm{Tg\,CO\,yr^{-1}})^{-1}$ (mean ± 1 standard deviation) (CV = 0.045), suggesting little variability. The greatest global annual net RFs result from the global CO reduction, followed by EA, IN, and AF reductions. When normalized per unit change in CO emissions, global annual net RF is most sensitive to regions close to the equator (ME, SE, and IN). This is consistent with the regions that produce the greatest changes in tropospheric O_3 burden per unit change in CO emissions, but the response for ME emissions is larger than expected given its O_3 burden change (Table 7, Table S9), due to the hotter and drier conditions of this region. By doubling the global annual net RF of the 50 % global CO reduction ($0.072\,\mathrm{W\,m^{-2}}$), we find that our estimated CO RF contribution is approximately 5 % of the global net RF of CO_2 ($1.56\,\mathrm{W\,m^{-2}}$), and smaller

ACPD
12, 33443–33488, 2012

than the RF of CO and NMVOC emissions in previous studies: $0.21 \pm 0.10\,W\,m^{-2}$ due to tropospheric O_3 and CH_4 changes (Shindell et al., 2005; Forster et al., 2007) and $0.25 \pm 0.04\,W\,m^{-2}$ when SO_4^{2-}, nitrate, and CO_2 contributions are included (Shindell et al., 2009). Among the positive forcing agents with short lifetimes (CO, CH_4, NMVOCs, and BC), CO RF is also ~5 % of the total RF (~ $1.57\,W\,m^{-2}$) (Forster et al., 2007).

Following the methods of Collins et al. (2012) and Fry et al. (2012), we estimate GWPs for each regional perturbation, at 20 and 100-yr time horizons (Table 8, Fig. 8). GWP_H estimates are calculated as the RF integrated to a time horizon H due to an emission pulse, normalized by the change in emissions, and divided by the equivalent for CO_2. Since O_3 RF has both short and long-term components, we calculate long-term O_3 RF by scaling the O_3 RF from the CH_4 control simulation by the ratio of long-term O_3 burden changes in each regional perturbation to those of the CH_4 control simulation. We then calculate short-term O_3 RF as the difference between steady-state and long-term O_3 RF. We assume that short-term RF components (SO_4^{2-} and short-term O_3) are constant over one year and then drop to zero instantaneously. Long-term components (CH_4 and long-term O_3) respond and decay with the calculated CH_4 perturbation lifetime (12.48 yr). Figure 8 shows the breakdown of total GWP into short and long-term components, and error bars representing the average uncertainty of CO GWPs (GWP_{20}: ± 1.4 and GWP_{100}: ± 0.5) from Fry et al. (2012) across multiple global CTMs (± 1 standard deviation). However, the error bars do not account for the full uncertainty, as additional forcings, such as from CO_2, are excluded, which may alter total net RF and GWP estimates. We estimate GWP_{20} and GWP_{100} values of 4.07 and 1.34, respectively, for the global CO reduction, and ranges of 3.71 to 4.37 (CV = 0.059) and 1.26 to 1.44 (CV = 0.043) among regions, suggesting little regional variability.

Our GWP_{100} estimates are comparable to those of Derwent et al. (2001) (GWP_{100} of 1.0 due to O_3 changes, and 0.6 due to CH_4 changes) and Daniel and Solomon (1998) (GWP_{100} of 1.0), yet smaller than the GWP_{100} estimates of Fuglestvedt et al. (1996) (GWP_{100} of 3.0) and Johnson and Derwent (1996) (GWP_{100} of 2.1). Our GWP_{20} and

ACPD
12, 33443–33488, 2012

GWP_{100} estimates are also about 65 to 70 % lower than those estimated by Berntsen et al. (2005) for Europe and East Asia, but those did not include SO_4^{2-} impacts as we do here, and 16 to 23 % lower than those estimated by Fry et al. (2012), likely due to differences among the CTMs, such as a lower sensitivity of O_3 and CH_4 to CO emissions in MOZART-4, but regional definitions also differ (Table S10). Although the absolute GWP estimates of Fry et al. (2012) are more robust than those presented here, reflecting an ensemble of CTMs, the present study more fully addresses the variability of GWPs over a wide range of regions encompassing the tropics and northern and southern extra-tropics.

As mentioned earlier, our GWP estimates do not include the forcing from CO_2 once CO oxidizes. This reflects the accounting of carbon emissions in CO_2 inventories (Fuglestvedt et al., 1996; Daniel and Solomon, 1998; Collins et al., 2002). If the CO_2 forcing were accounted for, the GWP_{100} and GWP_{20} estimates would each increase by 1.57 ($44\,g\,CO_2\,mol^{-1}$ $(28\,g\,CO\,mol^{-1})^{-1}$).

6 Conclusions

Reducing CO emissions can slow near-term climate change while improving air quality from O_3 and CO itself. The present-day CO RF is estimated as 5 % of that from CO_2, and also 5 % of the short-lived forcing agents that provide an opportunity to slow climate change in the coming decades. We find here that the global net RF of CO reductions varies little among the regions where it is emitted, but CO may cause changes in regional climate that were not quantified here.

Halving anthropogenic CO emissions globally and from 10 regions has widespread effects on surface and tropospheric concentrations in addition to net RF. For the global CO emission reduction, global annual net RF, GWP_{20}, and GWP_{100} estimates are $-0.124\,mW\,m^{-2}\,(Tg\,CO\,yr^{-1})^{-1}$, 4.07, and 1.34, respectively, with ranges of -0.115 to $-0.131\,mW\,m^{-2}\,(Tg\,CO\,yr^{-1})^{-1}$, 3.71 to 4.37, and 1.26 to 1.44 among the 10 regions, with regions in the tropics (ME, SE, and IN) having the greatest sensitivities. We find

ACPD
12, 33443–33488, 2012

little variability in the net RF and GWP estimates among source regions. Our GWP estimates agree well with previous studies (Daniel and Solomon, 1998; Derwent et al., 2001), but are less than the GWP_{20} and GWP_{100} estimates of Berntsen et al. (2005) and Fry et al. (2012), likely related to differences among CTMs. The GWP values should be increased by 1.57 for fossil fuel sources to account for the CO_2 generated as an oxidation product. However, care should be taken to avoid double counting, as CO_2 emissions are often calculated by assuming complete oxidation of the fuel rather than being measured in the exhaust. It is always preferable for climate to emit the carbon as CO_2 rather than CO.

Net RF distributions for the regional (and global) reductions show widespread cooling across the NH and SH corresponding to the patterns of regional short-term O_3 and global CH_4 (and long-term O_3) decreases, and localized positive and negative net RFs due to changes in SO_4^{2-} aerosols. The strongest annual net RFs occur within the tropics (28° S to 28° N), independent of the location of CO emissions change, due to higher temperatures and greater absorption of infrared radiation.

For all regional reductions, we show that the greatest changes in surface CO and O_3 concentrations are within the region of emissions change, with lesser decreases hemispherically. The regions with the highest anthropogenic CO emissions (EA, IN, AF, and NA) show the largest impacts on surface CO and O_3 concentrations within that region and between regions. The impact of EA's reduction on US surface CO and O_3 concentrations is 39 % and 93 %, respectively, of that resulting from NA. The NA CO reduction also has a strong impact on EU and ME surface O_3 concentrations.

All of the reductions increase tropospheric OH burdens leading to decreases in global CH_4 and hence, long-term O_3. At the same time, tropospheric H_2O_2 decreases in all cases. We generally find that increases in OH contribute to increases in SO_4^{2-} formation through gas-phase oxidation, which is dominant in drier regions and near the equator. Decreases in H_2O_2 and O_3 contribute to decreases in SO_4^{2-} formation via aqueous-phase oxidation, which prevails mostly in the northern mid-latitudes.

ACPD
12, 33443–33488, 2012

For all regional reductions, more than 70 % of the global O_3 burden and production changes, and more than 79 % of global CO burden changes, occur outside the reduction region. In addition, O_3 production changes outside the source region greatly exceed changes in O_3 export from each source region, suggesting that long-range O_3 impacts are influenced substantially by the transport of CO and subsequent production of O_3 downwind, and less by the transport of O_3 itself. Tropospheric O_3 burden changes (per unit change in CO emissions) are most sensitive to SE, IN, and AF reductions, due to stronger photochemistry and more active vertical convection in the tropics compared to other regions (Naik et al., 2005; West et al., 2009a).

Limitations of this study include only accounting for O_3, CH_4, and SO_4^{2-} changes in net RF and GWP estimates. We exclude changes in nitrate aerosols, secondary organic aerosols, stratospheric O_3, water vapor, the carbon cycle via O_3 and nitrogen deposition, and CO_2, as these components are not part of the current RTM configuration. Our RTM simulations also do not include the indirect effects of aerosols on clouds or the internal mixing of aerosols, but these effects may be large. We estimate only small changes in NH_4NO_3 and SOA, consistent with previous studies that show these aerosols contributing much less to CO RF than SO_4^{2-} (Shindell et al., 2009). Stratospheric O_3 and water vapor RFs are believed to be relatively small (Forster et al., 2007). The contribution of CO emissions to CO_2 RF via changes in the CO_2 uptake by plants is estimated as 12 and 42 % of the net RF (Fry et al., 2012), which would increase GWPs and perhaps the variability among regions, depending on regional vegetation distributions.

We do not assess climate responses as in Shindell and Faluvegi (2009), but show how the location of CO emissions affects the latitudinal distribution of net RF and CO GWPs. Regional CO emissions are also considered fairly uncertain (Duncan et al., 2007), according to a number of studies that have used inverse modeling or adjoint methods to constrain CO emissions by satellite data (Heald et al., 2004; Pétron et al., 2004, Pfister et al., 2004, 2005; Kopacz et al., 2009, 2010), but this uncertainty likely does not strongly influence normalized forcing and GWP estimates. Uncertainties in

ACPD
12, 33443–33488, 2012

the emissions of other O_3 precursors and in the chemical and transport processes of MOZART-4 are likewise important (Berntsen et al., 2005).

Future international climate agreements or emissions trading mechanisms could include CO among a suite of long-lived greenhouse gases, using a single GWP globally, given that the uncertainty in the global GWP for CO is greater than the range among regions estimated here. Alternatively, different GWPs could be applied to different continents. In either case, this work provides an incentive to reduce CO emissions, as part of coordinated policies addressing climate and air quality.

Supplementary material related to this article is available online at: http://www.atmos-chem-phys-discuss.net/12/33443/2012/acpd-12-33443-2012-supplement.pdf.

Acknowledgements. This research has been funded by the US EPA under the Science to Achieve Results (STAR) Graduate Fellowship Program (M. Fry), by the US EPA Office of Air Quality Planning and Standards, and by a UNC Junior Faculty Development award (J. J. West). EPA has not officially endorsed this report, and the views expressed herein may not reflect the views of EPA. We thank L. Emmons (UCAR) for observation comparison tools, L. Emmons and S. Walters (UCAR) for MOZART-4 guidance, and P. Dolwick and C. Jang (US EPA).

References

Akimoto, H.: Global air quality and pollution, Science, 302, 1716–1719, doi:10.1126/science.1092666, 2003.

Barth, M. C., Rasch, P. J., Kiehl, J. T., Benkovitz, C. M., and Schwartz, S. E.: Sulfur chemistry in the National Center for Atmospheric Research Community Climate Model: description, evaluation, features, and sensitivity to aqueous chemistry, J. Geophys. Res., 105, 1387–1415, 2000.

ACPD
12, 33443–33488, 2012

Bauer, S. E. and Menon, S.: Aerosol direct, indirect, semidirect, and surface albedo effects from sector contributions based on the IPCC AR5 emissions for preindustrial and present-day conditions, J. Geophys. Res., 117, D01206, doi:10.1029/2011JD016816, 2012.

Bauer, S. E., Koch, D., Unger, N., Metzger, S. M., Shindell, D. T., and Streets, D. G.: Nitrate aerosols today and in 2030: a global simulation including aerosols and tropospheric ozone, Atmos. Chem. Phys., 7, 5043–5059, doi:10.5194/acp-7-5043-2007, 2007.

Berntsen, T. K., Fuglestvedt, J. S., Joshi, M. M., Shine, K. P., Stuber, N., Ponater, M., Sausen, R., Hauglustaine, D. A., and Li, L.: Response of climate to regional emissions of ozone precursors: sensitivities and warming potentials, Tellus B, 57, 283–304, doi:10.1111/j.1600-0889.2005.00152.x, 2005.

Carlton, A. G., Bhave, P. V., Napelenok, S. L., Edney, E. O., Sarwar, G., Pinder, R. W., Pouliot, G. A., and Houyoux, M.: Model representation of secondary organic aerosol in CMAQv4.7, Environ. Sci. Technol., 44, 8553–8560, doi:10.1021/es100636q, 2010.

Chung, S. and Seinfeld, J.: Global distribution and climate forcing of carbonaceous aerosols, J. Geophys. Res., 107, 4407, doi:10.1029/2001JD001397, 2002.

Collins, W. J., Derwent, R. G., Johnson, C. E., and Stevenson, D. S.: The oxidation of organic compounds in the troposphere and their global warming potentials, Climatic Change, 52, 453–479, doi:10.1023/A:1014221225434, 2002.

Collins, W. J., Fry, M. M., Yu, H., Fuglestvedt, J. S., Shindell, D. T., and West, J. J.: Global and regional temperature-change potentials for near-term climate forcers, Atmos. Chem. Phys. Discuss., 12, 23261–23290, doi:10.5194/acpd-12-23261-2012, 2012.

Daniel, J. S. and Solomon, S.: On the climate forcing of carbon monoxide, J. Geophys. Res., 103, 13249–13260, doi:10.1029/98JD00822, 1998.

Duncan, B. N., Logan, J. A., Bey, I., Megretskaia, I. A., Yantosca, R. M., Novelli, P. C., Jones, N. B., and Rinsland, C. P.: The global budget of CO, 1988–1997: source estimates and validation with a global model, J. Geophys. Res., 112, D22301, doi:10.1029/2007JD008459, 2007.

Emmons, L. K., Walters, S., Hess, P. G., Lamarque, J.-F., Pfister, G. G., Fillmore, D., Granier, C., Guenther, A., Kinnison, D., Laepple, T., Orlando, J., Tie, X., Tyndall, G., Wiedinmyer, C., Baughcum, S. L., and Kloster, S.: Description and evaluation of the Model for Ozone and Related chemical Tracers, version 4 (MOZART-4), Geosci. Model Dev., 3, 43–67, doi:10.5194/gmd-3-43-2010, 2010.

ACPD
12, 33443–33488, 2012

Fiore, A. M., Jacob, D. J., Field, B. D., Streets, D. G., Fernandes, S. D., and Jang, C.: Linking ozone pollution and climate change: the case for controlling methane, Geophys. Res. Lett., 29, 1919, doi:10.1029/2002GL015601, 2002.

Fiore, A. M., West, J. J., Horowitz, L. W., Naik, V., and Schwarzkopf, M. D.: Characterizing the tropospheric ozone response to methane emission controls and the benefits to climate and air quality, J. Geophys. Res., 113, D08307, doi:10.1029/2007JD009162, 2008.

Fiore, A. M., Dentener, F. J., Wild, O., Cuvelier, C., Schultz, M. G., Hess, P., Textor, C., Schulz, M., Doherty, R. M., Horowitz, L. W., MacKenzie, I. A., Sanderson, M. G., Shindell, D. T., Stevenson, D. S., Szopa, S., Van Dingenen, R., Zeng, G., Atherton, C., Bergmann, D., Bey, I., Carmichael, G., Collins, W. J., Duncan, B. N., Faluvegi, G., Folberth, G., Gauss, M., Gong, S., Hauglustaine, D., Holloway, T., Isaksen, I. S. A., Jacob, D. J., Jonson, J. E., Kaminski, J. W., Keating, T. J., Lupu, A., Marmer, E., Montanaro, V., Park, R. J., Pitari, G., Pringle, K. J., Pyle, J. A., Schroeder, S., Vivanco, M. G., Wind, P., Wojcik, G., Wu, S., and Zuber, A.: Multimodel estimates of intercontinental source-receptor relationships for ozone pollution, J. Geophys. Res., 114, D04301, doi:10.1029/2008JD010816, 2009.

Forster, P. M. D. and Shine, K. P.: Radiative forcing and temperature trends from stratospheric ozone changes, J. Geophys. Res., 102, 10481–10857, doi:10.1029/96JD03510, 1997.

Forster, P., Ramaswamy, V., Artaxo, P., Berntsen, T., Betts, R., Fahey, D. W., Haywood, J., Lean, J., Lowe, D. C., Myhre, G., Nganga, J., Prinn, R., Raga, G., Schulz, M., and Van Dorland, R.: Changes in atmospheric constituents and in radiative forcing, in: Climate Change 2007: The Physical Science Basis. Contribution of Working Group I to the Fourth Assessment Report of the Intergovernmental Panel on Climate Change, edited by: Solomon, S., Qin, D., Manning, M., Chen, Z., Marquis, M., Averyt, K. B., Tignor, M., and Miller, H. L., Cambridge Univ. Press, Cambridge, UK, 129–234, 2007.

Fry, M. M., Naik, V., West, J. J., Schwarzkopf, M. D., Fiore, A. M., Collins, W. J., Dentener, F. J., Shindell, D. T., Atherton, C., Bergmann, D., Duncan, B. N., Hess, P., MacKenzie, I. A., Marmer, E., Schultz, M. G., Szopa, S., Wild, O., and Zeng, G.: The influence of ozone precursor emissions from four world regions on tropospheric composition and radiative climate forcing, J. Geophys. Res., 117, D07306, doi:10.1029/2011JD017134, 2012.

Fuglestvedt, J. S., Isaksen, I. S. A., and Wang, W.-C.: Estimates of indirect global warming potentials for CH_4, CO, and NO_x, Climate Change, 34, 405–437, 1996.

Fuglestvedt, J. S., Berntsen, T. K., Isaksen, I. S. A., Mao, H. T., Liang, X. Z., and Wang, W. C.: Climatic forcing of nitrogen oxides through changes in tropospheric ozone

ACPD
12, 33443–33488, 2012

and methane; global 3-D model studies, Atmos. Environ., 33, 961–977, doi:10.1016/S1352-2310(98)00217-9, 1999.
GFDL Global Atmospheric Model Development Team (GAMDT): The new GFDL global atmosphere and land model AM2-LM2: Evaluation with prescribed SST simulations, J. Climate, 17, 4641–4673, 2004.
Granier, C., Guenther, A., Lamarque, J., Mieville, A., Muller, J., Olivier, J., Orlando, J., Peters, J., Petron, G., Tyndall, G., and Wallens, S.: POET, a database of surface emissions of ozone precursors, available at: http://accent.aero.jussieu.fr/POET_metadata.php, 2005.
Guenther, A., Karl, T., Harley, P., Wiedinmyer, C., Palmer, P. I., and Geron, C.: Estimates of global terrestrial isoprene emissions using MEGAN (Model of Emissions of Gases and Aerosols from Nature), Atmos. Chem. Phys., 6, 3181–3210, doi:10.5194/acp-6-3181-2006, 2006.
Heald, C. L., Jacob, D. J., Fiore, A. M., Emmons, L. K., Gille, J. C., Deeter, M. N., Warner, J., Edwards, D. P., Crawford, J. H., Hamlin, A. J., Sachse, G. W., Browell, E. V., Avery, M. A., Vay, S. A., Westberg, D. J., Blake, D. R., Singh, H. B., Sandholm, S. T., Talbot, R. W., and Fuelberg, H. E.: Asian outflow and trans-Pacific transport of carbon monoxide and ozone pollution: an integrated satellite, aircraft and model perspective, J. Geophys. Res., 108, 4804, doi:10.1029/2003JD003507, 2003.
Heald, C. L., Jacob, D. J., Jones, D. B. A., Palmer, P. I., Logan, J. A., Streets, D. G., Sachse, G. W., Gille, J. C., Hoffman, R. N., and Nehrkorn, T.: Comparative inverse analysis of satellite (MOPITT) and aircraft (TRACE-P) observations to estimate Asian sources of carbon monoxide, J. Geophys. Res., 109, D15S04, doi:10.1029/2004JD005185, 2004.
Horowitz, L. W., Fiore, A. M., Milly, G. P., Cohen, R. C., Perring, A., Wooldridge, P. J., Hess, P. G., Emmons, L. K., and Lamarque, J.-F.: Observational constraints on the chemistry of isoprene nitrates over the eastern United States, J. Geophys. Res., 112, D12S08, doi:10.1029/2006JD007747, 2007.
Hoyle, C. R., Myhre, G., Berntsen, T. K., and Isaksen, I. S. A.: Anthropogenic influence on SOA and the resulting radiative forcing, Atmos. Chem. Phys., 9, 2715–2728, doi:10.5194/acp-9-2715-2009, 2009.
Jackson, S. C.: Parallel pursuit of near-term and long-term climate mitigation, Science, 326, 526–527, doi:10.1126/science.1177042, 2009.
Jacob, D. J.: Introduction to Atmospheric Chemistry, Princeton University Press, Princeton, NJ, 1999.

ACPD
12, 33443–33488, 2012

Johnson, C. E. and Derwent, R. G.: Relative radiative forcing consequences of global emissions of hydrocarbons, carbon monoxide, and NO_x from human activities estimated with a zonally-averaged two-dimensional model, Climatic Change, 34, 439–462, 1996.

Lacis, A. A., Wuebbles, D. J., and Logan, J. A.: Radiative forcing of climate by changes in the vertical distribution of ozone, J. Geophys. Res., 95, 9971–9981, doi:10.1029/JD095iD07p09971, 1990.

Lamarque, J.-F., Kiehl, J. T., Hess, P. G., Collins, W. D., Emmons, L. K., Ginoux, P., Luo, C., and Tie, X. X.: Response of a coupled chemistry-climate model to changes in aerosol emissions: global impact on the hydrological cycle and the tropospheric burdens of OH, ozone, and NO_x, Geophys. Res. Lett., 32, L16809, doi:10.1029/2005GL023419, 2005.

Lapina, K., Honrath, R. E., Owen, R. C., Martin, M. V., and Pfister, G.: Evidence of significant large-scale impacts of boreal fires on ozone levels in the midlatitude Northern Hemisphere free troposphere, Geophys. Res. Lett., 33, L10815, doi:10.1029/2006GL025878, 2006.

Lawrence, M. G.: Photochemistry in the tropical pacific troposphere: studies with a global 3-D chemistry-meteorology model, Ph.D. thesis, Georgia Institute of Technology, 1996.

Lawrence, M. G., Crutzen, P. J., Rasch, P. J., Eaton, B. E., and Mahowald, N. M.: A model for studies of tropospheric photochemistry: description, global distributions, and evaluation, J. Geophys. Res., 104, 26245–26277, 1999.

Lawrence, M. G., Jöckel, P., and von Kuhlmann, R.: What does the global mean OH concentration tell us?, Atmos. Chem. Phys., 1, 37–49, doi:10.5194/acp-1-37-2001, 2001.

Lawrence, M. G., von Kuhlmann, R., Salzmann, M., and Rasch, P. J.: The balance of effects of deep convective mixing on tropospheric ozone, Geophys. Res. Lett., 30, 1940, doi:10.1029/2003GL017644, 2003.

Leibensperger, E. M., Mickley, L. J., Jacob, D. J., and Barrett, S. R. H.: Intercontinental influence of NO_x and CO emissions on particulate matter air quality, Atmos. Environ., 45, 3318–3324, doi:10.1016/j.atmosenv.2011.02.023, 2011.

Liao, H. and Seinfeld, J. H.: Global impacts of gas-phase chemistry-aerosol interactions on direct radiative forcing by anthropogenic aerosols and ozone, J. Geophys. Res., 110, D18208, doi:10.1029/2005JD005907, 2005.

Meinshausen, M., Smith, S. J., Calvin, K. V., Daniel, J. S., Kainuma, M. L. T., Lamarque, J.-F., Matsumoto, K., Montzka, S. A., Raper, S. C. B., Riahi, K., Thomson, A. M., Velders, G. J. M., and van Vuuren, D.: The RCP greenhouse gas concentrations and their extension from 1765 to 2300, Climatic Change, 109, 213–241, doi:10.1007/s10584-011-0156-z, 2011.

ACPD
12, 33443–33488, 2012

Metzger, S., Dentener, F., Pandis, S., and Lelieveld, J.: Gas/aerosol partitioning: 1. a computationally efficient model, J. Geophys. Res., 107, 4312, doi:10.1029/2001JD001102, 2002.
Naik, V., Mauzerall, D., Horowitz, L., Schwarzkopf, M. D., Ramaswamy, V., and Oppenheimer, M.: Net radiative forcing due to changes in regional emissions of tropospheric ozone precursors, J. Geophys. Res., 110, D24306, doi:10.1029/2005JD005908, 2005.
Naik, V., Mauzerall, D. L., Horowitz, L. W., Schwarzkopf, M. D., Ramaswamy, V., and Oppenheimer, M.: On the sensitivity of radiative forcing from biomass burning aerosols and ozone to emission location, Geophys. Res. Lett., 34, L03818, doi:10.1029/2006GL028149, 2007.
Olivier, J., Peters, J., Granier, C., Petron, G., Muller, J., and Wallens, S.: Present and future surface emissions of atmospheric compounds, POET report #2, EU project EVK2-1999-00011, available at: http://accent.aero.jussieu.fr/POET_metadata.php, 2003.
Pétron, G., Granier, C., Khattatov, B., Yudin, V., Lamarque, J., Emmons, L., Gille, J., and Edwards, D. P.: Monthly CO surface sources inventory based on the 2000–2001 MOPITT satellite data, Geophys. Res. Lett., 31, L21107, doi:10.1029/2004GL020560, 2004.
Pham, M., Muller, J. F., Brasseur, G. P., Granier, C., and Megie, G.: A three-dimensional study of the tropospheric sulfur cycle, J. Geophys. Res., 100, 26061–26092, doi:10.1029/95JD02095, 1995.
Pfister, G., Pétron, G., Emmons, L. K., Gille, J. C., Edwards, D. P., Lamarque, J.-F., Attié, J.-L., Granier, C., and Novelli, P. C.: Evaluation of CO simulations and the analysis of the CO budget for Europe, J. Geophys. Res., 109, D19304, doi:10.1029/2004JD004691, 2004.
Pfister, G., Hess, P., Emmons, L., Lamarque, J.-F., Wiedinmeyer, C., Edwards, D., Pétron, G., Gille, J., and Sachse, G.: Quantifying CO emissions from the 2004 Alaskan wildfires using MOPITT CO data, Geophys. Res. Lett., 32, L11809, doi:10.1029/2005GL022995, 2005.
Pfister, G. G., Emmons, L. K., Hess, P. G., Honrath, R., Lamarque, J.-F., Val Martin, M., Owen, R. C., Avery, M. A., Browell, E. V., Holloway, J. S., Nedelec, P., Purvis, R., Ryerson, T. B., Sachse, G. W., and Schlager, H.: Ozone production from the 2004 North American boreal fires, J. Geophys. Res., 111, D24S07, doi:10.1029/2006JD007695, 2006.
Pfister, G. G., Emmons, L. K., Hess, P. G., Lamarque, J.-F., Orlando, J. J., Walters, S., Guenther, A., Palmer, P. I., and Lawrence, P. J.: Contribution of isoprene to chemical budgets: a model tracer study with the NCAR CTM MOZART-4, J. Geophys. Res., 113, D05308, doi:10.1029/2007JD008948, 2008.
Prather, M. J.: Time scales in atmospheric chemistry: theory, GWPs for CH_4 and CO, and runaway growth, Geophys. Res. Lett., 23, 2597–2600, doi:10.1029/96GL02371, 1996.

ACPD
12, 33443–33488, 2012

Prather, M., Ehhalt, D., Dentener, F., Derwent, R. G., Dlugokencky, E., Holland, E., Isaksen, I. S. A., Katima, J., Kirchhoff, V., Matson, P., Midgley, P. M., and Wang, M.: Climate Change 2001: The Scientific Basis, edited by: Houghton, J. T. et al., Cambridge Univ. Press, Cambridge, UK, 239–287, 2001.

Prather, M. J., Holmes, C. D., and Hsu, J. J.: Reactive greenhouse gas scenarios: systematic exploration of uncertainties and the role of atmospheric chemistry, Geophys. Res. Lett., 39, L09803, doi:10.1029/2012GL051440, 2012.

Ramaswamy, V., Boucher, O., Haigh, J., Hauglustaine, D., Haywood, J., Myhre, G., Nakajima, T., Shi, G. Y., and Solomon, S.: Radiative forcing of climate change, in: Climate Change 2001: The Scientific Basis. Contribution of Working Group I to the Third Assessment Report of the Intergovernmental Panel on Climate Change, edited by: Houghton, J. T., Ding, Y., Griggs, D. J., Noguer, M., Linden, P. J. v. d., Dai, X., Maskell, K., and Johnson, C. A., Cambridge University Press, Cambridge, UK and New York, NY, USA, 349–416, 2001.

Riahi, K., Gruebler, A., and Nakicenovic, N.: Scenarios of long-term socio-economic and environmental development under climate stabilization, Technol. Forecast. Soc., 74, 887–935, 2007.

Riahi, K., Rao, S., Krey, V., Cho, C., Chirkov, V., Fischer, G., Kindermann, G., Nakicenovic, N., and Rafaj, P.: RCP 8.5 – a scenario of comparatively high greenhouse gas emissions, Climatic Change, 109, 33–57, doi:10.1007/s10584-011-0149-y, 2011.

Rienecker, M. M., Suarez, M. J., Todling, R., Bacmeister, J., Takacs, L., Liu, H.-C., Gu, W., Sienkiewicz, M., Koster, R. D., Gelaro, R., Stajner, I., and Nielsen, J. E.: The GEOS-5 Data Assimilation System – Documentation of Versions 5.0.1, 5.1.0, and 5.2.0, NASA Tech. Memo., NASA/TM-2008-104606, vol. 27, 118 pp., 2008.

Rypdal, K., Berntsen, T., Fuglestvedt, J. S., Aunan, K., Torvanger, A., Stordal, F., Pacyna, J. M., and Nygaard, L. P.: Tropospheric ozone and aerosols in climate agreements: scientific and political challenges, Environ. Sci. Policy, 8, 29–43, doi:10.1016/j.envsci.2004.09.003, 2005.

Rypdal, K., Rive, N., Berntsen, T., Fagerli, H., Klimont, Z., Mideksa, T. K., and Fuglestvedt, J. S.: Climate and air quality-driven scenarios of ozone and aerosol precursor abatement, Environ. Sci. Policy, 12, 855–869, doi:10.1016/j.envsci.2009.08.002, 2009.

Saikawa, E., Naik, V., Horowitz, L. W., Liu, J. F., and Mauzerall, D. L.: Present and potential future contributions of sulfate, black and organic carbon aerosols from China to global air quality, premature mortality and radiative forcing, Atmos. Environ., 43, 2814–2822, doi:10.1016/j.atmosenv.2009.02.017, 2009.

ACPD
12, 33443–33488, 2012

Schultz, M. G., Backman, L., Balkanski, Y., Bjoerndalsaeter, S., Brand, R., Burrows, J. P., Dalsoeren, S., de Vasconcelos, M., Grodtmann, B., Hauglustaine, D. A., Heil, A., Hoelzemann, J. J., Isaksen, I. S. A., Kaurola, J., Knorr, W., Ladstaetter-Weißenmayer, A., Mota, B., Oom, D., Pacyna, J., Panasiuk, D., Pereira, J. M. C., Pulles, T., Pyle, J., Rast, S., Richter, A., Savage, N., Schnadt, C., Schulz, M., Spessa, A., Staehelin, J., Sundet, J. K., Szopa, S., Thonicke, K., van het Bolscher, M., van Noije, T., van Velthoven, P., Vik, A. F., Wittrock, F.: REanalysis of the TROpospheric chemical composition over the past 40 years (RETRO) – A long-term global modeling study of tropospheric chemistry, Final Report, Max Planck Institute for Meteorology, Jülich/Hamburg, Germany, ISSN 1614-1199, 2007.

Schwarzkopf, M. D. and Ramaswamy, V.: Radiative effects of CH_4, N_2O, halocarbons and the foreign-broadened H_2O continuum: a GCM experiment, J. Geophys. Res., 104, 9467–9488, doi:10.1029/1999JD900003, 1999.

Seinfeld, J. H., Erdakos, G. B., Asher, W. E., and Pankow, J. F.: Modeling the formation of secondary organic aerosol (SOA), 2, the predicted effects of relative humidity on aerosol formation in the a-pinene-, b-pinene-, sabinene-, d3-carene-, and cyclohexene-ozone systems, Environ. Sci. Technol., 35, 1806–1817, 2001.

Seinfeld, J. H. and Pandis, S. N.: Atmospheric Chemistry and Physics – From Air Pollution to Climate Change, 2nd Edn., John Wiley and Sons, Inc., Hoboken, NJ, ISBN 0471828572, 2006.

Shindell, D. T., Faluvegi, G., Stevenson, D. S., Krol, M. C., Emmons, L. K., Lamarque, J.-F., Pétron, G., Dentener, F. J., Ellingsen, K., Schultz, M. G., Wild, O., Amann, M., Atherton, C. S., Bergmann, D. J., Bey, I., Butler, T., Cofala, J., Collins, W. J., Derwent, R. G., Doherty, R. M., Drevet, J., Eskes, H. J., Fiore, A. M., Gauss, M., Hauglustaine, D. A., Horowitz, L. W., Isaksen, I. S. A., Lawrence, M. G., Montanaro, V., Müller, J.-F., Pitari, G., Prather, M. J., Pyle, J. A., Rast, S., Rodriguez, J. M., Sanderson, M. G., Savage, N. H., Strahan, S. E., Sudo, K., Szopa, S., Unger, N., van Noije, T. P. C., and Zeng, G.: Multimodel simulations of carbon monoxide: comparison with observations and projected near-future changes, J. Geophys. Res., 111, D19306, doi:10.1029/2006JD007100, 2006.

Shindell, D. and Faluvegi, G.: Climate response to regional radiative forcing during the twentieth century, Nat. Geosci., 2, 294–300, doi:10.1038/NGEO473, 2009.

Shindell, D. T., Faluvegi, G., Koch, D. M., Schmidt, G. A., Unger, N., and Bauer, S. E.: Improved attribution of climate forcing to emissions, Science, 326, 716–718, doi:10.1126/science.1174760, 2009.

ACPD
12, 33443–33488, 2012

Shindell, D., Kuylenstierna, J. C. I., Vignati, E., van Dingenen, R., Amann, M., Klimont, Z., Anenberg, S. C., Muller, N., Janssens-Maenhout, G., Raes, F., Schwartz, J., Faluvegi, G., Pozzoli, L., Kupiainen, K., Höglund-Isaksson, L., Emberson, L., Streets, D., Ramanathan, V., Hicks, K., Oanh, N. T. K., Milly, G., Williams, M., Demkine, V., and Fowler, D.: Simultaneously mitigating near-term climate change and improving human health and food security, Science, 335, 183–189, doi:10.1126/science.1210026, 2012.

Spivakovsky, C. M., Logan, J. A., Montzka, S. A., Balkanski, Y. J., Foreman-Fowler, M., Jones, D. B. A., Horowitz, L. W., Fusco, A. C., Brenninkmeijer, C. A. M., Prather, M. J., Wofsy, S. C., and McElroy, M. B.: Three-dimensional climatological distribution of tropospheric OH: update and evaluation, J. Geophys. Res., 105, 8931–8980, 2000.

Stevenson, D. S., Dentener, F. J., Schultz, M. G., Ellingsen, K., van Noije, T. P. C., Wild, O., Zeng, G., Amann, M., Atherton, C. S., Bell, N., Bergmann, D. J., Bey, I., Butler, T., Cofala, J., Collins, W. J., Derwent, R. G., Doherty, R. M., Drevet, J., Eskes, H. J., Fiore, A. M., Gauss, M., Hauglustaine, D. A., Horowitz, L. W., Isaksen, I. S. A., Krol, M. C., Lamarque, J.-F., Lawrence, M. G., Montanaro, V., Muller, J.-F., Pitari, G., Prather, M. J., Pyle, J. A., Rast, S., Rodriguez, J. M., Sanderson, M. G., Savage, N. H., Shindell, D. T., Strahan, S. E., Sudo, K., and Szopa, S.: Multimodel ensemble simulations of present-day and near-future tropospheric ozone, J. Geophys. Res., 111, D08301, doi:10.1029/2005JD006338, 2006.

Task Force on Hemispheric Transport of Air Pollution: Hemispheric Transport of Air Pollution, United Nations Economic Commission for Europe, Geneva, Switzerland, 2010.

Tilmes, S., Lamarque, J.-F., Emmons, L. K., Conley, A., Schultz, M. G., Saunois, M., Thouret, V., Thompson, A. M., Oltmans, S. J., Johnson, B., and Tarasick, D.: Technical Note: Ozonesonde climatology between 1995 and 2011: description, evaluation and applications, Atmos. Chem. Phys., 12, 7475–7497, doi:10.5194/acp-12-7475-2012, 2012.

Unger, N., Shindell, D. T., Koch, D. M., and Streets, D. G.: Cross influences of ozone and sulfate precursor emissions changes on air quality and climate, P. Natl. Acad. Sci. USA, 103, 4377–4380, doi:10.1073/pnas.0508769103, 2006.

Von Kuhlmann, R.: Photochemistry of Tropospheric Ozone, its Precursors and the Hydroxyl Radical: A 3-D-Modeling Study Considering Non-Methane Hydrocarbons, Ph.D. Thesis, Johannes Gutenberg-Universität Mainz, Mainz, Germany, 2001.

Voulgarakis, A., Naik, V., Lamarque, J.-F., Shindell, D. T., Young, P. J., Prather, M. J., Wild, O., Field, R. D., Bergmann, D., Cameron-Smith, P., Cionni, I., Collins, W. J., Dalsøren, S. B., Doherty, R. M., Eyring, V., Faluvegi, G., Folberth, G. A., Horowitz, L. W., Josse, B.,

ACPD
12, 33443–33488, 2012

McKenzie, I. A., Nagashima, T., Plummer, D. A., Righi, M., Rumbold, S. T., Stevenson, D. S., Strode, S. A., Sudo, K., Szopa, S., and Zeng, G.: Analysis of present day and future OH and methane lifetime in the ACCMIP simulations, Atmos. Chem. Phys. Discuss., 12, 22945–23005, doi:10.5194/acpd-12-22945-2012, 2012.

Wang, W. C., Zhuang, Y. C., and Bojkov, R. D.: Climatic implications of observed changes in ozone vertical distribution in the middle and high latitudes of the Northern Hemisphere, Geophys. Res. Lett., 20, 1567–1570, doi:10.1029/93GL01318, 1993.

West, J. J., Fiore, A. M., Naik, V., Horowitz, L. W., Schwarzkopf, M. D., and Mauzerall, D. L.: Ozone air quality and radiative forcing consequences of changes in ozone precursor emissions, Geophys. Res. Lett., 34, L06806, doi:10.1029/2006GL029173, 2007.

West, J. J., Naik, V., Horowitz, L. W., and Fiore, A. M.: Effect of regional precursor emission controls on long-range ozone transport – Part 1: Short-term changes in ozone air quality, Atmos. Chem. Phys., 9, 6077–6093, doi:10.5194/acp-9-6077-2009, 2009a.

West, J. J., Naik, V., Horowitz, L. W., and Fiore, A. M.: Effect of regional precursor emission controls on long-range ozone transport – Part 2: Steady-state changes in ozone air quality and impacts on human mortality, Atmos. Chem. Phys., 9, 6095–6107, doi:10.5194/acp-9-6095-2009, 2009b.

Wild, O., Prather, M. J., and Akimoto, H.: Indirect long-term global radiative cooling from NO_x emissions, Geophys. Res. Lett., 28, 9, 1719–1722, doi:10.1029/2000GL012573, 2001.

World Meteorological Organization: WMO Greenhouse Gas Bulletin: The State of Greenhouse Gases in the Atmosphere using Global Observations through 2005, Bulletin No. 1: March 2006, 2006.

ACPD
12, 33443–33488, 2012

Table 1. For the base simulation, total anthropogenic CO emissions by region, and regional (or global) annual average area-weighted surface O_3, SO_4^{2-}, and CO concentrations.

Reduction region	Total Anthropogenic CO emissions ($Tg\,yr^{-1}$)	Annual Average Surface O_3 (ppbv)	Annual Average Surface SO_4^{2-} ($\mu g\,m^{-3}$)	Annual Average Surface CO (ppbv)
NA	70.0	35.3	1.6	151.0
SA	24.5	24.8	0.7	147.4
EU	31.2	36.5	3.0	166.0
FSU	21.9	33.2	1.4	166.3
AF	86.9	30.0	0.9	172.9
IN	96.4	41.2	2.9	279.4
EA	152.9	42.4	4.3	235.0
SE	54.3	28.1	1.6	174.5
AU	2.9	22.8	0.5	101.9
ME	42.6	40.4	2.5	147.5
Global	584.7	26.2	1.0	122.7

ACPD
12, 33443–33488, 2012

Table 2. Source-receptor matrix of annual average surface CO concentration changes (ppbv), for the regional reduction simulations, with the United States (US) also defined as a receptor in addition to the 10 regions. The largest changes for each source reduction region are in bold.

	Receptor										
Source	NA	SA	EU	FSU	AF	IN	EA	SE	AU	ME	US
NA	−12.5	−0.69	−4.56	−4.07	−1.34	−1.75	−3.27	−1.17	−0.32	−3.36	**−19.3**
SA	−0.19	**−3.81**	−0.13	−0.13	−0.56	−0.32	−0.17	−0.45	−0.83	−0.18	−0.15
EU	−2.32	−0.31	**−18.3**	−4.96	−0.98	−0.85	−2.56	−0.63	−0.13	−3.90	−2.16
FSU	−2.05	−0.18	−3.66	**−9.70**	−0.47	−0.69	−2.96	−0.49	−0.08	−2.03	−1.88
AF	−1.05	−2.47	−0.87	−0.87	**−10.2**	−1.84	−1.11	−1.47	−1.58	−1.42	−0.95
IN	−1.93	−1.03	−1.82	−2.00	−2.21	**−75.5**	−4.23	−3.50	−0.57	−2.76	−1.97
EA	−7.08	−1.29	−6.53	−7.68	−2.36	−4.79	**−50.0**	−8.36	−0.73	−5.08	−7.52
SE	−0.82	−0.72	−0.74	−0.73	−0.90	−1.90	−1.48	**−8.96**	−0.73	−0.83	−0.83
AU	−0.01	−0.11	−0.01	−0.01	−0.07	−0.04	−0.01	−0.10	**−0.81**	−0.02	−0.01
ME	−1.65	−0.49	−2.33	−2.95	−1.69	−5.91	−2.51	−0.94	−0.22	**−13.7**	−1.66

ACPD
12, 33443–33488, 2012

Table 3. For the global and regional reduction simulations relative to the base, global annual mean burden changes in tropospheric and upper tropospheric (UT) steady-state O_3, tropospheric CH_4, SO_4^{2-}, NH_4NO_3, and SOA.

Reduction region	ΔO_3 (Tg yr^{-1})	ΔUT O_3 (Tg yr^{-1})	ΔCH_4 (ppbv)	ΔSO_4^{2-} (Gg yr^{-1})	ΔNH_4NO_3 (Gg yr^{-1})	ΔSOA (Gg yr^{-1})
NA	−0.64	−0.37	−9.1	−0.54	0.24	−0.11
SA	−0.21	−0.14	−3.2	−0.05	−0.003	−0.02
EU	−0.27	−0.15	−4.1	−0.37	0.19	−0.07
FSU	−0.19	−0.11	−2.9	−0.22	0.12	−0.05
AF	−0.80	−0.51	−10.9	0.03	−0.09	−0.06
IN	−0.93	−0.61	−11.5	0.48	−0.29	−0.17
EA	−1.38	−0.84	−19.4	−1.25	0.22	−0.43
SE	−0.56	−0.38	−6.6	−0.11	−0.04	−0.12
AU	−0.02	−0.01	−0.4	−0.01	0.001	−0.001
ME	−0.38	−0.23	−5.6	0.37	0.003	−0.09
Global	−5.39	−3.35	−73.0	−1.82	0.39	−1.11

ACPD
12, 33443–33488, 2012

Table 4. For the global and regional reduction simulations, global annual mean changes in short-term surface O_3, steady-state surface O_3, steady-state surface O_3 per unit change in CO emissions, and long-term surface O_3 per unit change in CO emissions.

Reduction region	Δ Short-term surface O_3 (pptv)	Δ Steady-state surface O_3 (pptv)	Δ Steady-state surface O_3 per Tg CO emissions (pptv (Tg CO yr^{-1})$^{-1}$)	Δ Long-term surface O_3 per Tg CO emissions (pptv (Tg CO yr^{-1})$^{-1}$)
NA	−42.8	−63.0	−1.8	−0.58
SA	−8.7	−15.9	−1.3	−0.59
EU	−22.1	−31.2	−2.0	−0.58
FSU	−16.0	−22.4	−2.1	−0.58
AF	−31.3	−55.4	−1.3	−0.55
IN	−40.8	−66.4	−1.4	−0.53
EA	−77.8	−120.8	−1.6	−0.56
SE	−19.9	−34.5	−1.3	−0.54
AU	−1.2	−2.2	−1.5	−0.68
ME	−24.1	−36.5	−1.7	−0.58
Global	−287.8	−450.1	−1.5	−0.56

ACPD
12, 33443–33488, 2012

Table 5. Source-receptor matrix of annual average steady-state changes in surface O_3 concentrations (pptv), for the regional reduction simulations, with the United States (US) also defined as a receptor in addition to the 10 regions. The largest changes for each source reduction region are in bold.

	Receptor										
Source	NA	SA	EU	FSU	AF	IN	EA	SE	AU	ME	US
NA	−178.2	−26.0	−131.1	−97.3	−46.8	−71.5	−102.4	−35.1	−20.7	−119.6	**−253.3**
SA	−14.4	**−25.3**	−14.2	−11.9	−16.4	−17.5	−15.6	−12.9	−15.2	−17.1	−15.4
EU	−48.4	−11.3	**−170.8**	−68.9	−24.7	−32.9	−57.9	−16.4	−9.1	−91.5	−56.0
FSU	−36.9	−7.6	−58.3	**−75.1**	−14.5	−25.8	−53.3	−12.1	−6.3	−50.9	−43.5
AF	−59.8	−52.1	−59.6	−49.9	**−97.2**	−77.2	−66.4	−46.0	−41.5	−77.7	−64.1
IN	−85.0	−37.6	−89.0	−76.8	−66.9	**−454.6**	−129.2	−67.2	−30.7	−114.5	−96.0
EA	−197.0	−53.4	−209.2	−178.2	−90.5	−158.6	**−437.7**	−118.9	−45.7	−202.0	−235.7
SE	−41.5	−24.3	−42.6	−35.6	−34.5	−57.0	−52.3	**−57.9**	−24.0	−50.0	−46.4
AU	−1.6	−1.9	−1.6	−1.4	−1.9	−2.1	−1.8	−2.0	**−4.8**	−2.0	−1.7
ME	−49.7	−17.1	−63.4	−59.0	−38.4	−105.9	−69.1	−25.0	−13.4	**−159.3**	−57.5

ACPD
12, 33443–33488, 2012

Table 6. For each regional reduction, changes in global annual average (short-term) tropospheric CO burden (B_{CO}), and B_{CO} per unit change in CO emissions (E_{CO}). Also shown are CO lifetime calculated as $\Delta B_{CO}/(\Delta E_{CO} + \Delta P_{CO})$, the fractions of B_{CO} change outside each reduction region and in the UT, and the changes in net CO export (X_{CO}) from the reduction region, global CO production (P_{CO}), and P_{CO} outside the reduction region. The total global annual average CO burden in the base simulation is 462.6 Tg CO.

Reduction region	ΔB_{CO} short-term (Tg CO)	$\Delta B_{CO}/\Delta E_{CO}$ (days)	CO Lifetime (days)	Fraction of ΔB_{CO} outside region	Fraction of ΔB_{CO} in UT	ΔX_{CO} from region (Tg yr^{-1})	ΔP_{CO} global (Tg yr^{-1})	ΔP_{CO} outside region (Tg yr^{-1})
NA	−6.7	70.3	78.2	0.82	0.37	−27.4	3.5	2.7
SA	−2.5	74.0	82.2	0.88	0.41	−10.4	1.2	1.0
EU	−3.4	79.3	88.2	0.92	0.30	−13.7	1.6	1.4
FSU	−2.5	83.7	93.1	0.79	0.29	−9.1	1.1	0.95
AF	−7.9	66.2	73.4	0.83	0.44	−33.6	4.3	3.3
IN	−8.0	60.5	66.7	0.92	0.45	−40.2	4.5	3.8
EA	−14.7	70.1	77.7	0.90	0.39	−64.6	7.5	6.5
SE	−4.9	66.4	73.4	0.89	0.50	−23.4	2.6	2.2
AU	−0.3	84.2	94.1	0.92	0.35	−1.3	0.2	0.14
ME	−4.0	68.2	75.8	0.90	0.36	−17.8	2.1	1.8

ACPD
12, 33443–33488, 2012

Table 7. Changes in global annual average (short-term) tropospheric O_3 burden (B_{O_3}), O_3 production (P_{O_3}), and net O_3 export (X_{O_3}) from each regional reduction, normalized per change in CO emissions (E_{CO}), and the fractions of these above each reduction region and in the upper troposphere (UT). Regional O_3 lifetimes are also shown. The total global annual average O_3 burden in the base simulation is 352.2 Tg O_3.

Reduction region	ΔB_{O_3} (Tg O_3) short-term	$\Delta B_{O_3}/\Delta E_{CO}$ (days)	ΔP_{O_3} (Tg yr^{-1})	$\Delta P_{O_3}/\Delta E_{CO}$ (Tg O_3 (Tg CO yr^{-1})$^{-1}$)	Regional O_3 lifetime ($\Delta B_{O_3}/\Delta P_{O_3}$) (days)	Fraction of global ΔB_{O_3} above region	Fraction of global ΔP_{O_3} above region	Fraction of global ΔP_{O_3} in UT	ΔX_{O_3} from region (Tg yr^{-1})	ΔP_{O_3} outside region (Tg yr^{-1})
NA	−0.413	4.31	−8.19	−0.234	18.4	0.14	0.30	0.37	−0.91	−5.75
SA	−0.135	4.02	−2.48	−0.202	19.9	0.07	0.17	0.50	−0.12	−2.06
EU	−0.168	3.93	−3.63	−0.233	16.9	0.05	0.18	0.30	−0.34	−2.98
FSU	−0.120	4.00	−2.53	−0.231	17.3	0.13	0.19	0.31	−0.13	−2.06
AF	−0.533	4.48	−9.59	−0.221	20.3	0.12	0.29	0.50	−1.02	−6.83
IN	−0.652	4.94	−11.0	−0.229	21.5	0.04	0.22	0.50	−1.26	−8.67
EA	−0.902	4.31	−16.8	−0.220	19.6	0.06	0.20	0.41	−1.58	−13.4
SE	−0.395	5.31	−6.19	−0.228	23.3	0.05	0.17	0.59	−0.40	−5.15
AU	−0.014	3.49	−0.27	−0.188	18.6	0.05	0.14	0.41	−0.01	−0.24
ME	−0.247	4.23	−4.98	−0.234	18.1	0.08	0.24	0.36	−0.47	−3.78

ACPD
12, 33443–33488, 2012

Table 8. Annual net RF globally and by latitude band ($mW\,m^{-2}$) and total GWP_{20} and GWP_{100} estimates for the regional and global reduction simulations relative to the base simulation, due to changes in tropospheric steady-state O_3, CH_4, and SO_4^2 concentrations. Global annual net shortwave radiation, net longwave radiation, and net RF per unit change in CO emissions $(mW\,m^{-2}\ (Tg\,CO\,yr^{-1})^{-1})$ are also shown. The 10 regions estimates represent the sum of the net RFs from all 10 regional reductions; these estimates are not directly estimated by the RTM.

Reduction region	Global annual net RF	Global annual net shortwave radiation	Global annual net longwave radiation	Global annual net RF per Tg CO	Annual net RF 90° S–28° S	Annual net RF 28° S–28° N	Annual net RF 28° N–60° N	Annual net RF 60° N–90° N	Total GWP_{20}	Total GWP_{100}
NA	−4.25	−0.31	−3.94	−0.122	−2.69	−6.20	−4.76	−3.32	3.98	1.33
SA	−1.51	−0.10	−1.40	−0.123	−1.04	−2.39	−1.45	−0.88	4.04	1.35
EU	−1.79	−0.07	−1.71	−0.114	−1.20	−2.70	−1.72	−1.36	3.71	1.26
FSU	−1.28	−0.07	−1.21	−0.117	−0.85	−1.89	−1.34	−1.00	3.78	1.28
AF	−5.46	−0.55	−4.92	−0.126	−3.61	−8.89	−5.25	−3.11	4.18	1.37
IN	−6.21	−0.85	−5.36	−0.129	−3.60	−10.0	−6.90	−3.70	4.34	1.41
EA	−9.12	−0.61	−8.50	−0.119	−5.80	−13.4	−10.3	−6.71	3.91	1.31
SE	−3.51	−0.34	−3.17	−0.129	−2.21	−5.79	−3.47	−1.99	4.34	1.41
AU	−0.18	−0.004	−0.17	−0.121	−0.12	−0.28	−0.18	−0.11	3.94	1.35
ME	−2.80	−0.40	−2.40	−0.131	−1.68	−4.36	−3.16	−1.81	4.37	1.44
GLOB	−36.1	−3.25	−32.9	−0.124	−22.8	−56.0	−38.6	−24.1	4.07	1.34
10 regions	−36.1	−3.31	−32.8	–	−22.8	−55.9	−38.6	−24.0	–	–

ACPD
12, 33443–33488, 2012

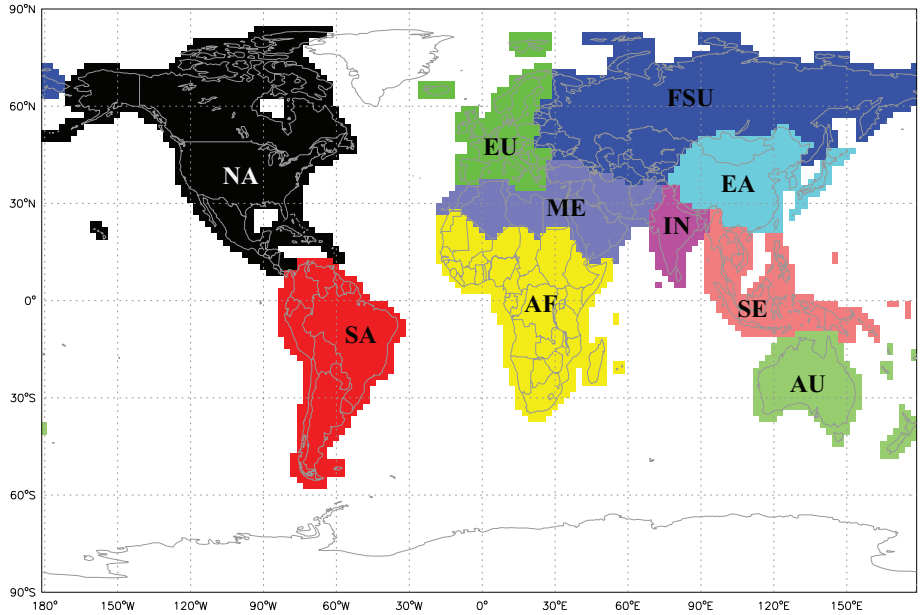

Fig. 1. Definition of 10 reduction regions.

ACPD
12, 33443–33488, 2012

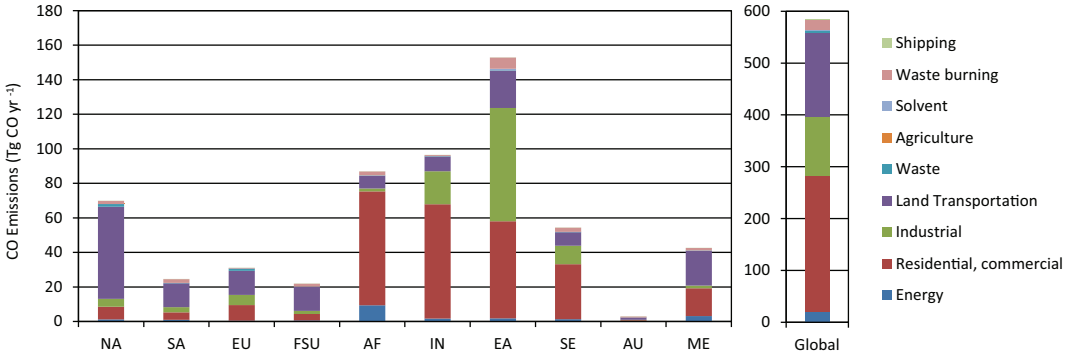

Fig. 2. Annual average anthropogenic CO emissions (Tg CO yr^{-1}) by region and sector for the base simulation, from the RCP8.5 emissions inventory for the year 2005.

ACPD
12, 33443–33488, 2012

Net RF and air quality responses of CO emissions

M. M. Fry

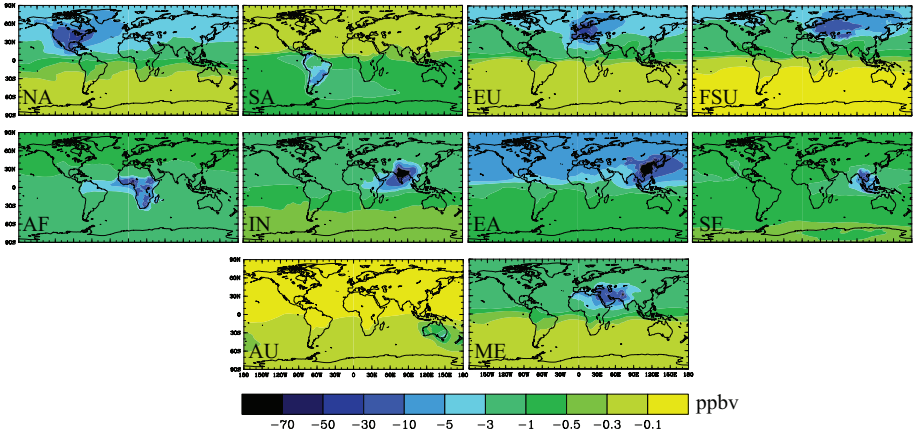

Fig. 3. Global distribution of annual average surface CO concentration changes (ppbv) for each of the regional reduction simulations relative to the base.

ACPD
12, 33443–33488, 2012

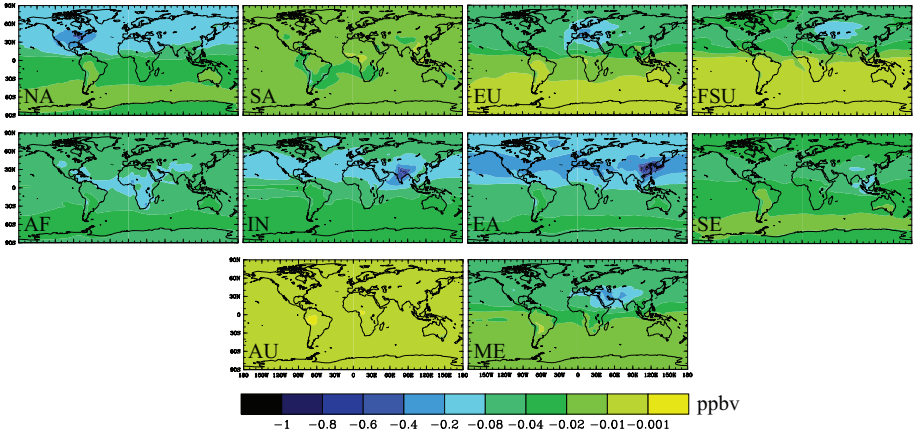

Fig. 4. Global distribution of annual average steady-state surface O_3 concentration changes (ppbv) for each of the regional reduction simulations relative to the base.

ACPD
12, 33443–33488, 2012

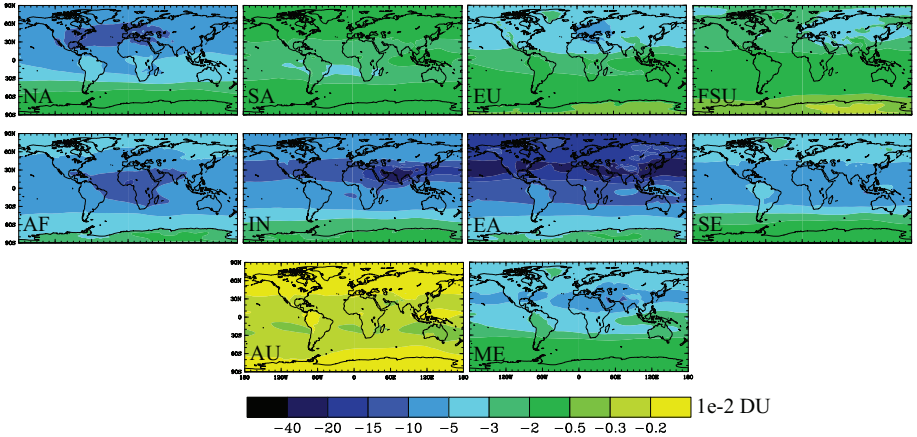

Fig. 5. Global distribution of annual average changes in tropospheric total column O_3 at steady state (1e-2 DU) for each of the regional reduction simulations relative to the base.

ACPD
12, 33443–33488, 2012

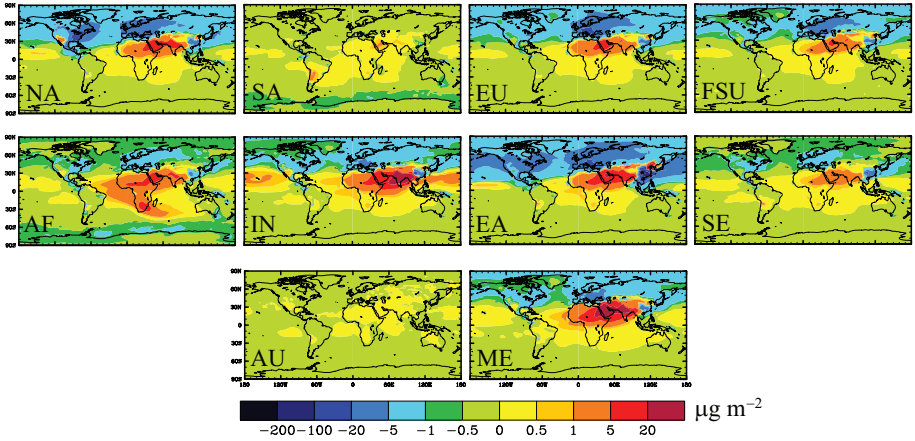

Fig. 6. Global distribution of annual average changes in tropospheric total column SO_4^{2-} ($\mu g\,m^{-2}$) for each of the regional reduction simulations relative to the base.

ACPD
12, 33443–33488, 2012

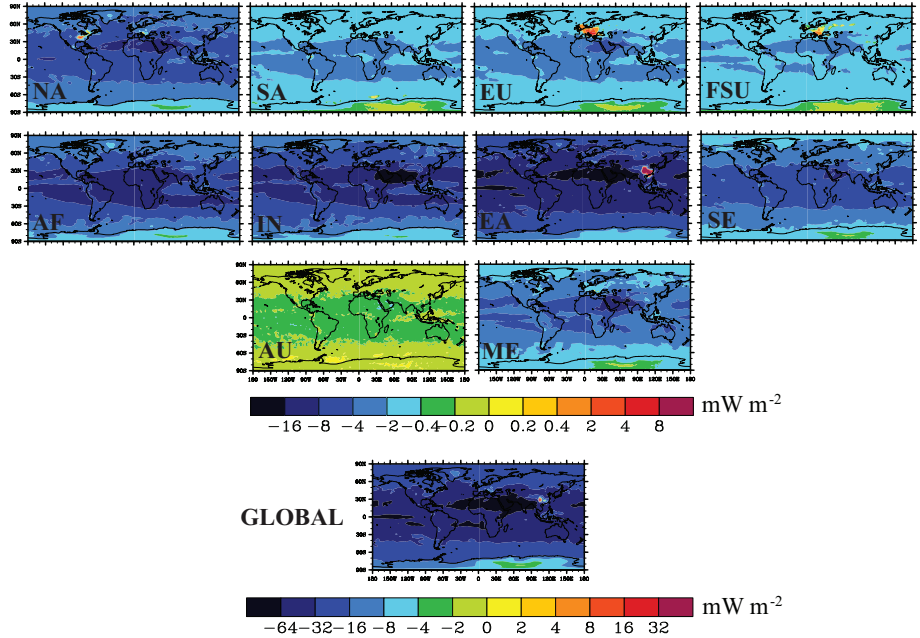

Fig. 7. Annual average net RF distributions ($mW\,m^{-2}$) due to changes in tropospheric steady-state O_3, CH_4, and SO_4^{2-} for the regional and global CO reduction simulations minus the base simulation. Note the difference in scale between the regional and global reductions.

ACPD
12, 33443–33488, 2012

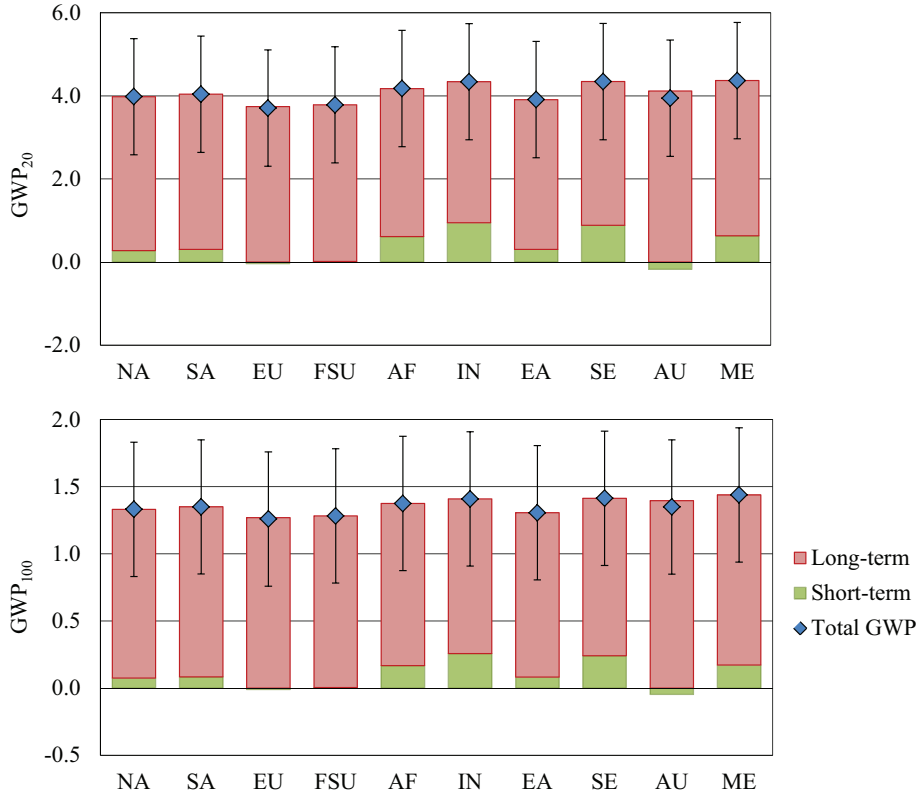

Fig. 8. Global warming potentials for CO at time horizons of 20 and 100 yr (GWP_{20}, GWP_{100}) for each regional reduction, and the contributions from short-term (O_3 and SO_4^{2-} changes) and long-term (long-term O_3 and CH_4) components. Uncertainty bars represent the average uncertainty found by Fry et al. (2012) based on the spread of atmospheric chemical models (1 standard deviation).

ACPD
12, 33443–33488, 2012